Image Restoration of Landscape Design Based on DCGAN Optimization Algorithm

Wenjun Zhang*
School of Architecture and Urban Planning, Henan University of Urban Construction, Pingdingshan 467036, China

***Abstract*—To enhance the quality and effectiveness of image restoration in landscape design, this study optimizes the existing methods for low efficiency and incomplete feature extraction in processing high-resolution and detail rich landscape design images. Firstly, based on the traditional generative adversarial network (GAN), a novel deep convolutional generative adversarial network (DCGAN) model is proposed. Subsequently, the model's ability to extract detailed features was enhanced by integrating dense connected networks (DenseNet) and compressed excitation networks (SENet) into the network architecture. An improved DCGAN is designed for the restoration of landscape design images. According to the results, the optimized model had a restoration precision and repair recall rate of 0.97 in benchmark performance testing, which was significantly better than traditional deep convolutional generative adversarial network models. In practical applications, the model had an average accuracy of over 97% in repairing four different styles of landscape images, with an average repair time as low as 0.06s. From this, it can be seen that the designed model can provide a more efficient technical means for the restoration and digital preservation of landscape design images.**

***Keywords*—Deep convolutional generative adversarial network; image; restoration; landscape architecture; squeeze-and-excitation network; dense convolutional network**

I. Introduction

Influenced by social economy and urbanization, landscape design has gradually become important in urban planning. As a crucial component of urban green infrastructure, landscape architecture not only exerts a crucial function in beautifying the environment and improving ecology, but also has a significant impact on enhancing the quality of life of citizens and the cultural taste of the city [1-2]. However, landscape design images with a long history are often eroded by environmental factors, resulting in image damage and information loss, which affects the research and protection of landscape architecture and challenges its ability of digital preservation and inheritance.

The damaged landscape art images not only affect the research and protection of landscape architecture, but also pose challenges to the digital preservation and inheritance of landscape architecture [3-4]. Generative Adversarial Networks (GANs) have demonstrate strong potential and broad application prospects in image generation and restoration. Traditional image restoration methods mainly rely on manual or rule-based techniques, which often inadequate when dealing with complex scenes and details. In contrast, GAN can effectively capture complex texture and structural features in images through adversarial training mechanisms of generators and discriminators, achieving high-quality image generation and restoration.

However, traditional GAN still faces some specific challenges in landscape image restoration. First of all, in the training process, traditional GAN often has the problem of high training difficulty, and its training process is easily affected by mode collapse and instability, resulting in unstable image quality. Secondly, traditional image restoration techniques are often inadequate in processing complex textures and detailed features, and cannot fully retain the fine features and details in high-resolution landscape design images [5-6]. The main goal of this study is to improve the quality and effectiveness of landscape design image restoration by improving the traditional GAN optimization algorithm, especially in the aspects of feature extraction and restoration efficiency.

Therefore, a deep Convolutional generative adversarial network (DCGAN) model combining DenseNet and SENet is proposed. This new model aims to enhance the ability of the network to extract detailed features, so as to achieve more accurate image recovery in practical applications. The research innovatively introduces Dense Connected Convolutional Networks (DenseNet) and Squeeze-and-Excitation Networks (SENet) as generators, and uses Deep Convolutional Generative Adversarial Networks (DCGAN) as discriminators, ultimately enabling the constructed model to extract more detailed features, reduce computational complexity, and effectively restore the original image. The potential benefit of the research is that the successful implementation of this approach will have a profound impact in several fields. First of all, in urban planning and management, high-quality image restoration can provide more accurate visual basis for decision-making and support more effective land use and environmental design. Secondly, in the field of cultural heritage protection, it can help preserve and restore historical documents and artistic works to ensure the long-term preservation and transmission of cultural heritage. Finally, in the practice of digital preservation, the research results can provide strong technical support for the maintenance of various digital archives and promote the sustainable management and utilization of digital content.

The structure of this paper is divided into six sections. Section II, literature review, summarizes the achievements and shortcomings of domestic image restoration research. Section III introduces the proposed method, including the DCGAN architecture and the integration of DenseNet and SENet, to improve image restoration performance. Section IV presents the experimental results, verifies the performance of the model, and compares the performance of DS-DCGAN with other models. Section V discusses the advantages and potential

applications of DS-DCGAN. Finally, the research contributions were summarized and future research directions were proposed in Section VI.

II. Related Works

GAN is a deep learning approach, which includes a generator and a discriminator, which can generate realistic data through adversarial training between the two. Image restoration adopts computer technology to restore damaged or degraded images, to improve image quality or restore their original state. In image restoration, Liu G et al. designed an image restoration algorithm on the basis of GAN to address the low accuracy of traditional algorithms in restoring large-area damaged images. By extracting multi-scale edge details of the damaged area and constructing a GAN model, the model was trained to generate the best fake image. The results showed that the model could effectively combine contextual and perceptual information, significantly improve image restoration accuracy and image quality, and outperform existing algorithms [7]. In response to the significant impact of equipment and operators on the quality of retinal images, Deng Z et al. explored the retinal image restoration method in real clinical environments. Firstly, a clinical dataset Real Fundus was established, which included 120 pairs images. Secondly, a Transformer-based GAN was proposed to restore the clinical fundus images. The proposed model was helpful for in-depth analysis of clinical fundus images [8]. Yang J et al. proposed a new approach for restoring private facial images on the basis of semantic features and adversarial samples to address the serious threat posed by facial image feature leakage to user information security. Firstly, Segnet network was used for semantic segmentation of facial images, and then GAN was used to generate adversarial samples and perturb the semantic features of facial images. Compared with other advanced technologies, the generated private facial images had stronger median filtering defense capability [9].

In response to the limitations of Wasserstein-GAN in simulating complex distributions such as natural image distributions, Ma H et al. proposed a method to improve Wasserstein-GAN training by introducing pairwise constraints to optimize image restoration tasks. The research results showed that the Wasserstein-GAN model with paired constraints had better consistency and perceptual quality than existing technical methods [10]. Considering that artworks can be damaged over time due to changes in humidity, temperature, and improper storage, Kumar P et al. designed a new virtual restoration strategy for artworks based on GAN. This method adopted an improved U-Net as the generator part. A pre-trained residual network was used to construct the encoder to generate higher quality feature embeddings, improving the quality of image restoration. The research results indicated that this method performed well in performance indicators [11]. Liang M et al. designed a multi-scale self attention GAN to address the common local cross contamination or data loss in the acquisition and processing of pathological digital images. Then this network was applied to restore pathological images of tissue. The research results showed that this network structure could achieve pixel level realistic restoration of tissue pathological images, effectively restoring the detailed features of the images [12].

In summary, although the existing GAN optimization algorithm has made some progress in the field of image restoration, it still has shortcomings in processing high-resolution and detail-rich landscape design images. Therefore, a DCGAN model combining DenseNet and SENet optimization is proposed in this paper, which aims to further improve the quality and effect of image restoration by improving the structure of generator and discriminator. Compared with the current methods, the research method has improved the efficiency of feature extraction and processing. Traditional GAN models often face the problem of insufficient feature extraction when processing complex landscape design images, especially when recovering high-resolution images, fine texture and structural features are easy to ignore. By integrating DenseNet, DS-DCGAN can realize the close connection of features, so that the network can use the feature information from different levels more effectively, and enhance the ability to extract detailed features. At the same time, the introduction of SENet optimizes the channel incentive mechanism and makes the network focus more on important features by adaptively adjusting the weight of the feature map. This channel attention mechanism significantly improves the ability of the generator and discriminator to respond to key features, thereby reducing unnecessary computational overhead while maintaining image quality. Compared with traditional DCGAN, DS-DCGAN has been optimized by deep learning technology to reduce the computational complexity and improve the overall operating efficiency.

III. Landscape Image Restoration based on Improved DCGAN

To improve the restoration effect of landscape images, the DCGAN is first introduced to generate clear landscape images. Secondly, a new generative network is generated by combining DenseNet and SENet, and DCGAN is used as the discriminative network to compensate for the insufficient feature extraction of traditional DCGAN models in repairing landscape images.

A. Design of Landscape Image Restoration Algorithm Based on DCGAN

GAN is a deep learning model proposed in 2014, which introduces two networks, namely a generator and a discriminator, so that these two networks compete with each other during the training process to generate realistic data [13]. The generator is to produce fake data that is close to the true data distribution. It obtains a random noise vector as input and outputs a data point with the same dimension as the training data. The discriminator is to distinguish whether the input data is real or generated by a generator. It can receive data produced by the generator or real data as input and output a probability value to represent the probability that the input data is real. The GAN is displayed in Fig. 1.

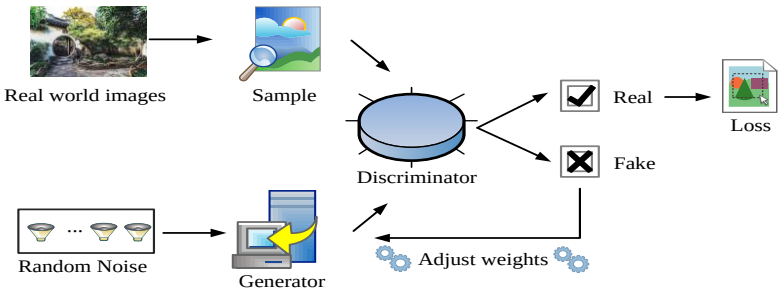

Fig. 1. GAN structure.

In Fig. 1, when training GAN, the generator first receives a random noise vector as input, and then uses this noise to generate a fake image, with the aim of making this image visually indistinguishable from the real image. Next, the discriminator may receive a fake image or a real image generated by the generator, and output a probability value to determine whether the image is real or produced by the generator. Through this adversarial learning, the generator gradually improves its ability to generate high-quality fake images to deceive the discriminator. The discriminator is constantly improving its accuracy in distinguishing between real and fake images. The dynamic confrontation between the two drives the continuous improvement of their performance until the generator can generate images that are almost unrecognizable as fake by the discriminator, while the discriminator accurately identifies the real and generated images as much as possible. The objective loss function of GAN is displayed in Eq. (1) [14-15].

$$\min_G \max_D V(D,G) = E_{x\sim p_{data}}[\log D(x)] + E_{z\sim p_z(z)}[\log(1-D(G(z)))] \quad (1)$$

In Eq. (1), G signifies the generator. D signifies the discriminator. z represents noise. x and $G(z)$ signify real samples and produced samples. $D(x)$ and $G(x)$ signify the discriminant function and the generative function, respectively. E represents the expected value. p_{data} and $p_z(z)$ represent the real and the produced distributions. $D(G(z))$ signifies the probability that D will distinguish the data generated by G as real samples. According to Eq. (1), to train GAN, G and D are trained separately. The training process of D is shown in Eq. (2).

$$\max_D V(D,G) = E_{x\sim p_{data}}[\log D(x)] + E_{z\sim p_z(z)}[\log(1-D(G(z)))] \quad (2)$$

In Eq. (2), the meanings of x and z are the same as those in Eq. (1). At this point, if D can recognize x as a true sample, then the value of $\log D(x)$ will be larger. Similarly, if D can identify $G(z)$ as a false sample, then the value of $\log(1-D(G(z)))$ will also be as large as possible. When the values of $\log D(x)$ and $\log(1-D(G(z)))$ are both larger, D remains unchanged and G is trained to confuse D. Similarly, when training G, it is hoped that D in GAN cannot recognize false samples. The training process of G is displayed in Eq. (3).

$$\min_G V(D,G) = E_{z\sim p_z(z)}[\log(1-D(G(z)))] \quad (3)$$

In Eq. (3), the closer the $D(G(z))$ is to 1, the smaller the training value of the entire G. DCGAN is a special type of GAN that combines the advantages of GAN and convolutional neural networks. Convolutional layers are used to construct generators and discriminators, enabling the network to obtain local and global features and generate more refined and realistic images. Firstly, in DCGAN, stride convolution is used in the discriminator to reduce image size, while fractional stride convolution is used in the generator to increase image size. Two convolution methods are shown in Fig. 2.

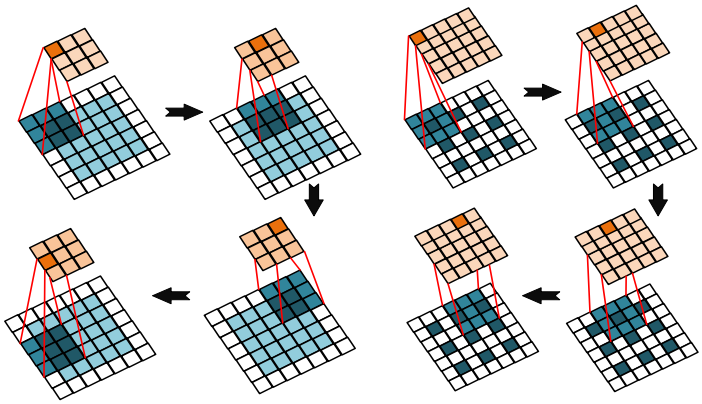

(a) Stride convolution (b) Fractional stride convolution

Fig. 2. The convolution processes of stride convolution and fractional stride convolution.

Fig. 2(a) and 2(b) show the convolution processes of stride convolution and fractional stride convolution, respectively. In Fig. 2(a), stride convolution reduces the output feature map size by setting the convolutional kernel movement step size. In ordinary convolution operations, the convolution kernel typically slides over the input feature map at stride of 1, resulting in output feature maps of the same size. However, by setting a larger stride value, such as 2 or 3, the convolution kernel will skip multiple pixels each time it slides on the input feature map, effectively reducing its size. This operation not only reduces computational complexity, but also has a down-sampling effect to some extent, allowing subsequent layers to process smaller feature maps, and improving the efficiency of the network. In Fig. 2(b), fractional stride convolution, also known as transpose convolution or deconvolution. This type of convolution is applied to increase the size of the output feature map. Unlike stride convolution, fractional stride convolution inserts zero padding before the convolution operation, allowing the convolution kernel to produce larger output feature maps than the original size when sliding on the input feature map. This operation essentially involves inserting blank spaces between input feature maps, and then performing standard convolution on the expanded image to increase its size. The DCGAN structure combining these two convolution operations is shown in Fig. 3.

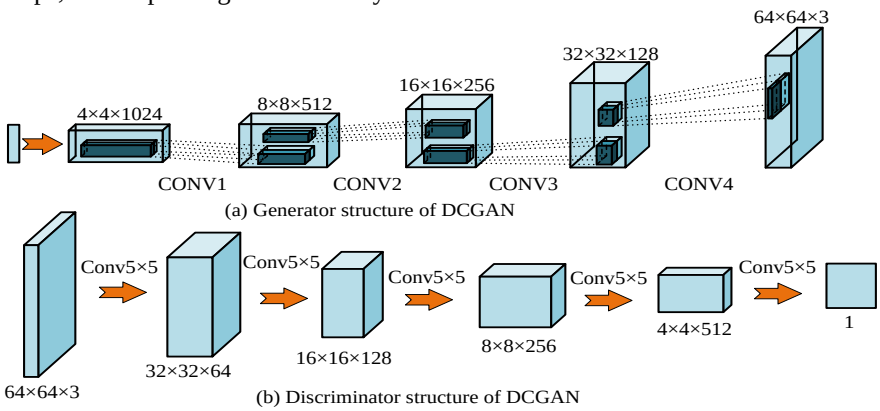

Fig. 3. DCGAN structure diagram.

The DCGAN in Fig. 3 consists of two main parts, namely the generator in Fig. 3(a) and the discriminator in Fig. 3(b). Among them, the former produces fake images. The later distinguishes between real images and generated fake images. The process of using DCGAN for image restoration includes the following key steps. Firstly, the generator takes a random noise vector as input and gradually enlarges the feature map through fractional stride convolutional layers, converting the noise into a fake image. Secondly, the discriminator will receive fake and real images generated by the generator, gradually reduce the size of the feature map through stride convolution layers, extract key features of the image, and output a probability value to represent the possibility that the input image is a real image. In this process, the generator and discriminator are continuously optimized through adversarial training. The generator attempts to generate increasingly realistic images to deceive the discriminator. The discriminator continuously distinguishes between real and fake images. After multiple rounds of iterative training, the generator is able to generate high-quality and realistic images, achieving the image restoration.

B. Construction of an Optimized DCGAN Model Combining DenseNet and SENet

Although DCGAN has better image feature extraction capabilities compared with GAN, there are still some shortcomings in using DCGAN for landscape design image restoration, such as unstable image quality, easy pattern collapse, high training difficulty, and poor feature extraction of some landscape images [16-17]. To address these issues, the DenseNet is combined with SENet to optimize the DCGAN. The structure of DenseNet is shown in Fig. 4.

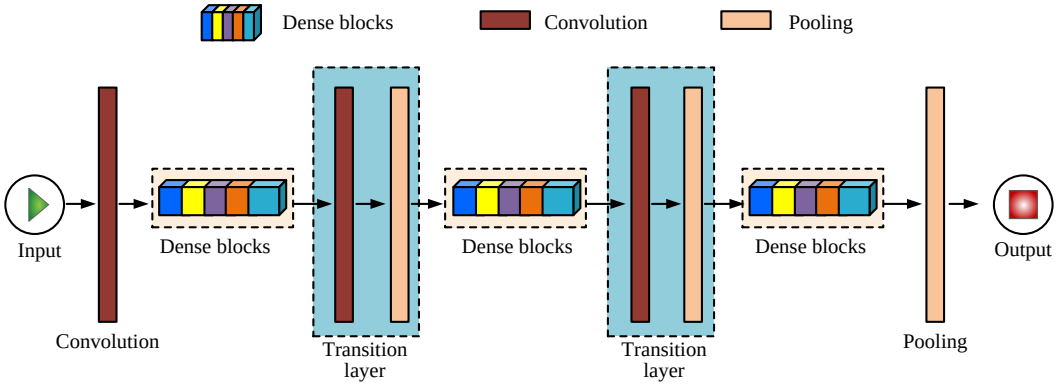

Fig. 4. DenseNet structure diagram.

The DenseNet in Fig. 4 is an innovative CNN structure characterized by the added densely connected modules. DenseNet consists of multiple dense convolutional blocks and transition layers. The layers in each dense convolutional block are directly connected to each other, meaning that the output of each preceding layer is the input of all subsequent layers. This design not only efficiently utilizes feature information, but also alleviates the gradient vanishing, thereby improving network performance. Another significant feature of DenseNet is to implement down-sampling through transition layers. The bottleneck layer in the transition layer can remove redundant information by reducing the number of feature maps, thereby reducing computational complexity and decreasing the parameters. x_0 represents the feature map obtained after convolution processing, which is the input of the dense convolution block to obtain the l-th layer output, as shown in Eq. (4) [18-19].

$$x_l = H_l\left(\left[x_0, x_1, \cdots, x_{l-1}\right]\right) \tag{4}$$

In Eq. (4), $H_l(\cdot)$ represents the transformation function of the l-th layer. $[x_0, x_1, \cdots, x_{l-1}]$ signifies the feature input composed of feature maps from layer 0 to $l-1$. x_l signifies the output of the l-th layer. In addition to using DenseNet to optimize the parameters of DCGAN and reduce the frequency of gradient vanishing, the study also adds SENet module to enhance channel sensitivity and lightweight the DCGAN structure. The SENet is displayed in Fig. 5.

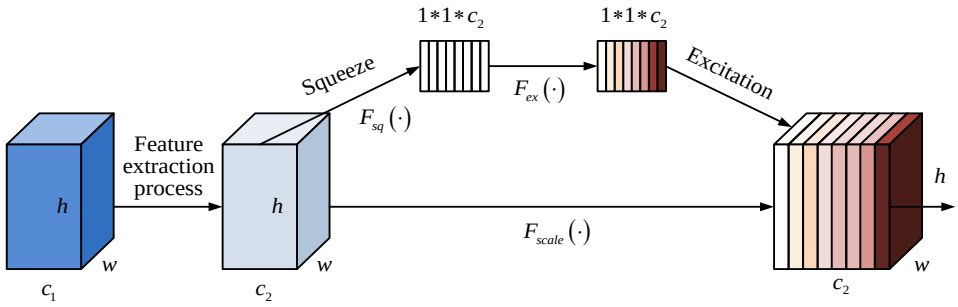

Fig. 5. SENet structure diagram.

In Fig. 5, the key component in the SENet structure is the excitation module, which can perform Squeeze and Excitation operations on the feature maps of the convolutional layer. Firstly, the feature map is compressed into a single value through global average pooling, which represents the global spatial information of the entire feature map. Then, this value is passed through a Fully Connected Layer (FCL) and ReLU function is used to learn the interrelationships between channels. Finally, this value through another FCL, and the Sigmoid is applied to output the weights of each channel. These weights will be used to re-weight the channels of the original feature map. The weights obtained through the incentive module will be multiplied with the corresponding channels to achieve feature re-calibration. After the above processing, the network can adaptively emphasize important features and suppress unimportant features. In the Squeeze operation, the original image feature size is $H*W*C$, where H, W, and C signify the height, width, and channels. Each channel is subjected to a global mean pooling operation to obtain a compressed feature map, which not only has a global receptive field but also has a size of $1*1*C$. The Squeeze operation is shown in Eq. (5).

$$z_c = F_{sq}\left(u_c\right) = \frac{1}{H \times W}\sum_{i=1}^{H}\sum_{j=1}^{W} u_c\left(i, j\right) \tag{5}$$

In Eq. (5), z_c signifies the compressed feature map. u_c represents the feature map extracted by convolution operation. $F_{sq}(\cdot)$ represents the feature compression function. i and j represent the horizontal and vertical axes of the feature map, respectively. The expression for the Excitation operation is shown in Eq. (6).

$$s_c = F_{ex}\left(z, W'\right) = \sigma\left(g\left(z, W'\right)\right) = \sigma\left(W_2 \operatorname{Re} LU\left(W_1 z\right)\right) \tag{6}$$

In Eq. (6), s_c represents the weight coefficient with attention mechanism. $F_{ex}(\cdot)$ represents the characteristic excitation function. z represents the compressed feature map. g represents the gating function. σ represents the reshape function. W', W_1 and W_2 respectively represent the weight coefficients of the attention mechanism, the first FCL, and the second FCL. The weight coefficients obtained through Squeeze and Excitation operations are applied to each channel, as shown in Eq. (7).

$$x_c = F_{scale}\left(u_c, s_c\right) \tag{7}$$

In Eq. (7), $F_{scale}(\cdot)$ represents the feature re-scaling function. x_c represents the weight coefficients applied to each channel. The DCGAN optimized by combining DenseNet and SENet is referred to as DS-DCGAN, and its structure is shown in Fig. 6.

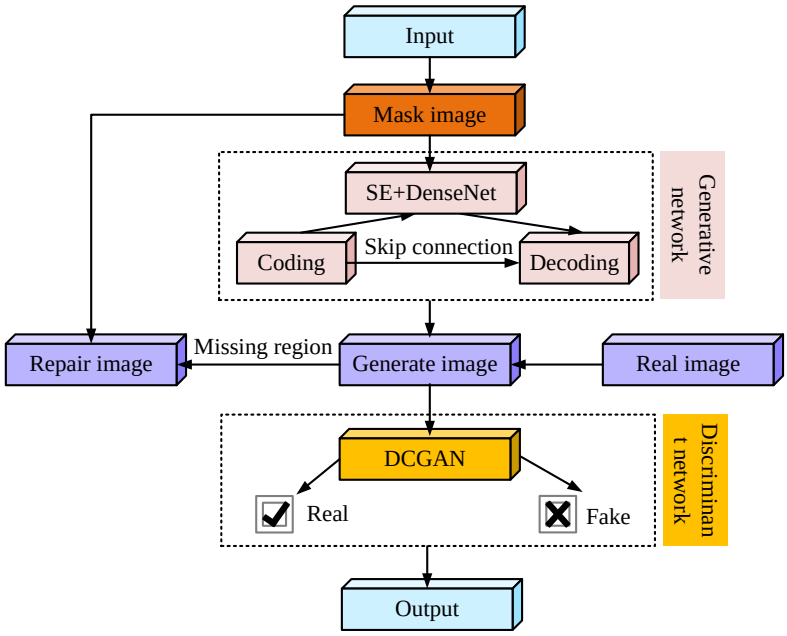

Fig. 6. DS-DCGAN structure.

In Fig. 6, the entire DS-DCGAN structure has the generator and the discriminator. DenseNet organizes the convolutional layers in a densely connected manner, meaning that each layer is directly connected to all the layers above it. In the generator, this dense connection can effectively transmit feature information, reduce information loss, and enable the network to better retain detailed features when generating images. The structure of DenseNet effectively alleviates the common phenomenon of gradient disappearance in deep networks. Since each layer is directly connected to the others, gradients can be passed more smoothly through the layers, ensuring that the generator can quickly learn effective feature representations during training. In the discriminator, by connecting the features of the front layer with the back layer, DenseNet can maximize the use of the features extracted from the front layer and form a stronger feature representation to judge the authenticity of the image. This enhanced feature utilization capability greatly improves the performance of the discriminator, which can more accurately distinguish the real image from the generated image. SENet enables the network to adaptively re-calibrate each channel by introducing a channel attention mechanism. Specifically, SENet acquires a global feature representation for each channel through global average pooling and generates channel weights through two fully connected layers. These weights are used to realign the importance of each channel in the input feature map. In the generator, the introduction of SENet enables the generated images to better highlight important feature channels, thus making the details of the generated images richer and more realistic. In the discriminator, SENet can effectively enhance the perception of key feature channels, making the discriminator pay more attention to the key features that may distinguish between real and generated images. SENet reduces the computational complexity and avoids the processing of meaningless features by cutting out unimportant feature channels. This not only improves computational efficiency, but also helps reduce overfitting and improves the network's ability to generalize on unseen data. In the DS-DCGAN structure, the loss function during training is shown in Eq. (8).

$$Loss_{train} = \lambda_{MSE} L_{MSE} + \lambda_{adv} L_{adv} + \lambda_{TV} L_{TV} \quad (8)$$

In Eq. (8), $Loss_{train}$, L_{MSE}, L_{adv}, and L_{TV} respectively represent the training set loss function, Mean Squared Error (MSE) function, adversarial loss function, and total variation loss function. λ_{MSE}, λ_{adv} and λ_{TV} represent the weights corresponding to the MSE function, adversarial loss function, and total variation loss function, respectively. The L_{MSE} is displayed in Eq. (9).

$$L_{MSE} = \left(x - G\left(M \otimes x\right)\right)^2 \quad (9)$$

In Eq. (9), M represents the binary mask. $\otimes$ represents multiplication between corresponding elements, while the meanings of other parameters remain consistent with those mentioned earlier. The L_{adv} is shown in Eq. (10).

$$L_{adv} = \log\left(D\left(x\right)\right) + \log\left(G\left(M \otimes x\right)\right) \quad (10)$$

In Eq. (10), the meanings of each parameter remain consistent with the previous text. The L_{TV} is shown in Eq. (11).

$$L_{TV} = \sum_{i,j} \left| G_{i+1,j}\left(M \otimes x\right) - G_{i,j}\left(M \otimes x\right) \right| + \left| G_{i,j+1}\left(M \otimes x\right) - G_{i,j}\left(M \otimes x\right) \right| \quad (11)$$

In Eq. (11), i and j still represent the horizontal-axis and longitudinal-axis of the feature map. The test set loss function is shown in Eq. (12).

$$L_{val} = \lambda_{context} L_{context} + \lambda_{prior} L_{prior} \quad (12)$$

In Eq. (12), L_{val}, $L_{context}$, and L_{prior} represent the training set loss function, text loss function, and prior loss function, respectively. $\lambda_{context}$ and λ_{prior} represent the weights of $L_{context}$ and L_{prior}, respectively.

IV. Restoration Effect Testing of Landscape Design Images based on DS-DCGAN

To exhibit the effectiveness of the DS-DCGAN model, the study selects DCGAN, Generative Adversarial Network-variant (GAN-variant), and Conditional GAN (CGAN) as comparison models. The benchmark performance and actual application effects of the four models are compared.

A. DS-DCGAN Model Benchmark Performance Testing

To validate the benchmark performance of the DS-DCGAN, two publicly available datasets for landscape architecture and landscape image restoration are selected for testing. Among them, the Places2 dataset contains over 10 million images of various natural scenes and buildings, widely used for image restoration and generation tasks. The Paris StreetView dataset contains high-resolution images of street view buildings, suitable for evaluating the performance of models in landscape architecture and landscape image restoration. The two datasets are separated into training and testing sets in an 8:2 to comprehensively assess the effectiveness and robustness in different types of image restoration tasks. The loss function value is used as a criterion to determine the stability of the model. The stability of the four models in two datasets is shown in Fig. 7.

Fig. 7(a) and 7(b) show the loss curves of CGAN, DCGAN, GAN-variant, and DS-DCGAN models. According to Fig. 7(a), CGAN, DCGAN, GAN-variant, and DS-DCGAN reached a stable state after 325, 278, 251, and 216 iterations, respectively. Similarly, in Fig. 7(b), CGAN, DCGAN, GAN-variant, and DS-DCGAN also reached a stable state after 296, 268, 223, and 172 iterations, respectively. Based on the two sub-graphs in Fig. 7, DS-DCGAN can iterate to a stable state faster compared with the other three comparison models, indicating its high training efficiency and strong adaptability of the model. The average time consumption of the four models in the decoding and encoding process is compared, as shown in Fig. 8.

Fig. 8(a) and 8(b) show the average encryption time and average decryption time of the four models during the training process, respectively. Based on Fig. 8, the CGAN model during training was 0.63 and 0.70, respectively. Its encryption and decryption process took the longest time, far higher than the DS-DCGAN model. In addition, the GAN-variant model was 0.35, the DCGAN model was 0.46 and 0.48, respectively, and the DS-DCGAN model was 0.21 and 0.19, respectively. Overall, the DS-DCGAN model has the shortest encryption and decryption time and the highest processing efficiency in image processing. The MSE and Mean Absolute Error (MAE) during the training process are displayed in Fig. 9.

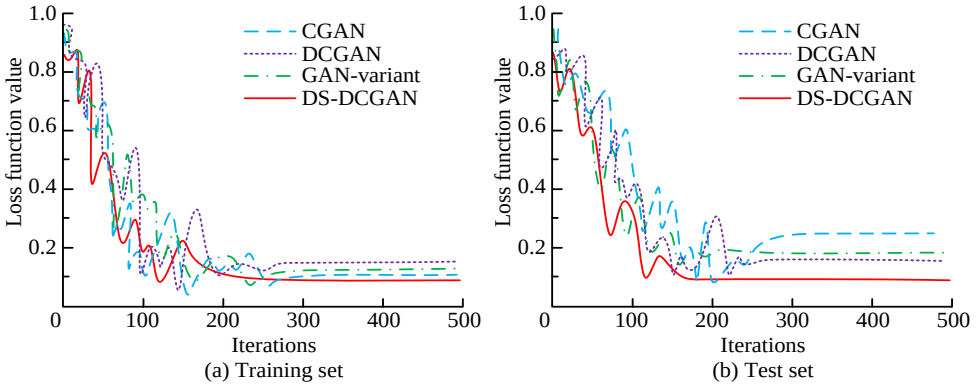

Fig. 7. Loss curve iteration of different models in two datasets.

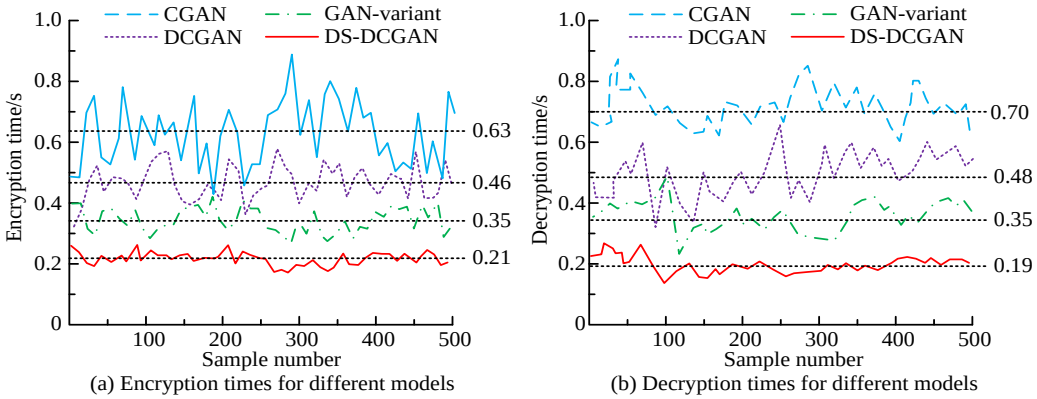

Fig. 8. Average encryption time and decryption time of various models.

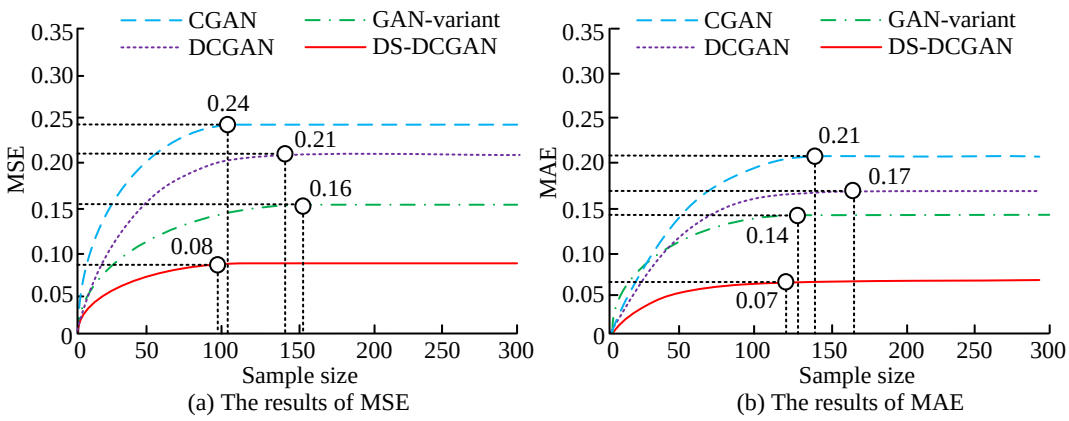

(a) The results of MSE (b) The results of MAE

Fig. 9. Error representation of different models.

Fig. 9(a) and Fig. 9(b) respectively show the MSE and MAE values of the four models. MSE is a common index to measure the difference between the restored image and the real image, and is defined as the average of the square of the difference between the pixel values of the corresponding position of the restored image and the original image. MAE is another measure of the difference between the recovered image and the real image, and it is the average of the absolute values of the difference between the pixel values. According to Fig. 9(a), the MSE values of CGAN, DCGAN, GAN-variant, and DS-DCGAN models after reaching stability were 0.24, 0.21, 0.16, and 0.08, respectively. According to Fig. 9(b), the MAE values of CGAN, DCGAN, GAN-variant, and DS-DCGAN models after reaching stability were 0.21, 0.17, 0.14, and 0.07, respectively. Overall, the DS-DCGAN model performs better in terms of error during training, with lower MSE and MAE values. The repair precision and recall values during the training are compared, as displayed in Fig. 10.

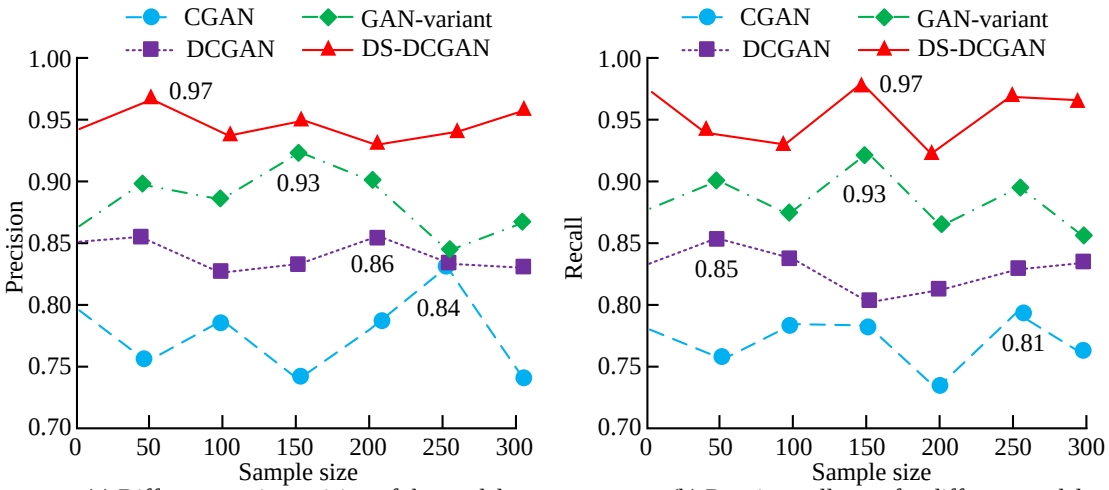

(a) Different repair precision of the model (b) Repair recall rates for different models

Fig. 10. Repair precision and repair recall rate of different models.

Fig. 10(a) and Fig. 10(b) respectively show the repair accuracy and repair recall rate of CGAN, DCGAN, GAN-variant and DS-DCGAN. The repair accuracy is used to evaluate the accuracy of images recovered by the model, and it represents the ratio of the number of pixels successfully recovered to the total number of pixels. The repair recall rate reflects the ability of the model to identify and recover the actual damaged part, and it represents the ratio of the true positives of successful recovery to the actual damaged part. In Fig. 10(a), the maximum repair precision of CGAN, DCGAN, GAN-variant, and DS-DCGAN was 0.84, 0.86, 0.93, and 0.97, respectively. In Fig. 10(b), the maximum repair recall rate of CGAN, DCGAN, GAN-variant, and DS-DCGAN was 0.81, 0.85, 0.93, and 0.97, respectively. From this, the benchmark performance test results of DS-DCGAN are good, which has high repair precision and recall.

B. *Application Effect Analysis of DS-DCGAN in Landscape Design Image Restoration*

In addition to comparing the benchmark performance of several models, the study also applies four models to practical problems. The application effects in landscape design image restoration are compared. Four different styles of landscape images are selected as the research objects. The restoration time and accuracy of four models for restoring these four real landscape images are obtained, as shown in Table I.

TABLE I. ACTUAL REPAIR EFFECT OF THE MODEL

Image Type	Evaluation index	CGAN	DCGAN	GAN-variant	DS-DCGAN
Image 1	Repair time /s	0.36	0.21	0.14	0.08
	Repair accuracy rate /%	88.23	91.05	95.18	98.15
Image 2	Repair time /s	0.31	0.23	0.18	0.11
	Repair accuracy rate /%	89.94	92.10	96.65	98.57
Image 3	Repair time /s	0.25	0.16	0.09	0.06
	Repair accuracy rate /%	89.69	92.17	95.04	99.03
Image 4	Repair time /s	0.41	0.30	0.24	0.15
	Repair accuracy rate /%	85.74	89.43	93.38	97.96

According to Table I, the repair time for four images using the DS-DCGAN model was controlled within 0.20s, with a minimum of 0.06s required to complete the repair work. At the same time, the accuracy of repairing images 1, 2, 3, and 4 based on the DS-DCGAN model was higher than that of comparison models, reaching 98.15%, 98.57%, 99.03%, and 97.96%, respectively. Among the four models, the CGAN model has the worst performance in practical applications, with a repair time of up to 0.41s and a repair accuracy of only 85.74%. The restoration effects of four models on real landscape images are further compared, as shown in Fig. 11.

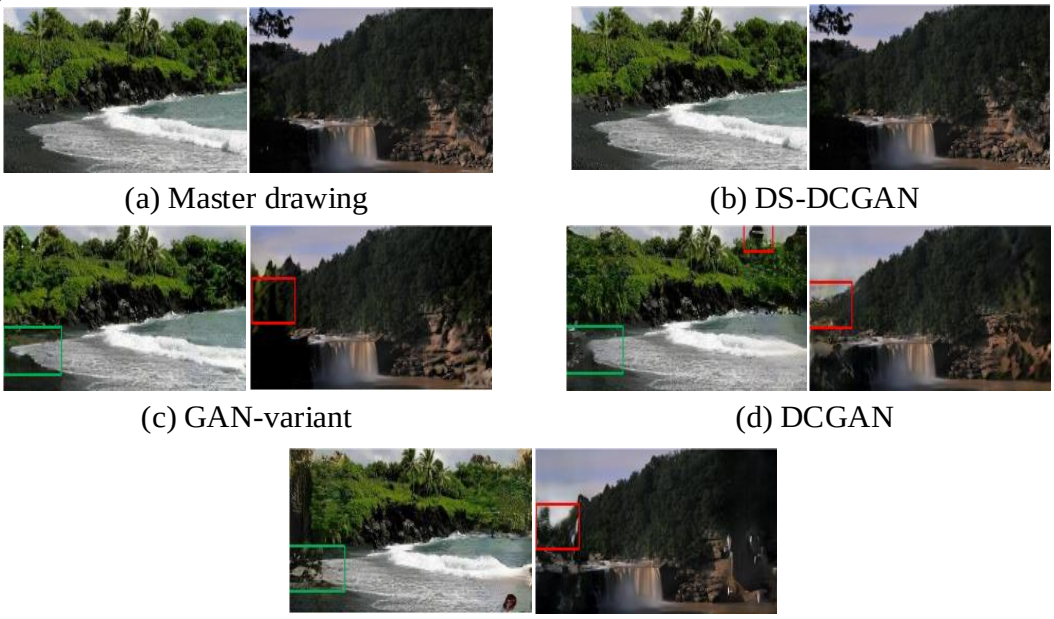

(a) Master drawing (b) DS-DCGAN

(c) GAN-variant (d) DCGAN

(e) CGAN

Fig. 11. Actual restoration effects of landscape design images under different models.

Fig. 11 shows the effectiveness of four models in restoring actual landscape design images. Based on Fig. 11, the CGAN, DCGAN, and GAN-variant models all generated features that did not match the original image when repairing images, while DS-DCGAN fully restored the true situation of the actual image without problems such as feature transfer or feature duplication. Overall, DS-DCGAN has the best restoration effect in practical applications. Based on the analysis of experimental results, the performance of the research method is shown in Table II.

TABLE II. PERFORMANCE RESULTS OF DS-DCGAN MODEL

Model	Repair accuracy (%)	Repair recall rate (%)	MSE	MAE	Average repair time (s)
CGAN	84	81	0.24	0.21	0.63
DCGAN	86	85	0.21	0.17	0.46
GAN-variant	93	93	0.16	0.14	0.35
DS-DCGAN	97	97	0.08	0.07	0.19

In Table II, DS-DCGAN's repair accuracy and recall rate are both as high as 97%, demonstrating excellent capabilities in detail recovery and extraction of important data. The high repair accuracy and recall rate indicate that DS-DCGAN is able to

capture critical information in images more comprehensively, thus providing more reliable image recovery results. DS-DCGAN has a MSE and MAE of 0.08 and 0.07, respectively, which are the lowest of all models and significantly reduce errors during image recovery. This shows that DS-DCGAN is able to reconstruct the original image more accurately, retaining more detailed information. The average repair time of DS-DCGAN is 0.19 seconds, which makes DS-DCGAN have good real-time performance in practical applications, especially suitable for scenarios that require fast recovery. The results show that DS-DCGAN provides higher recovery accuracy and speed, and provides effective support for practical applications that need to process high-definition images or large-scale data sets. Using DenseNet and SENet structure optimization, the model not only shows strong ability in processing complex image features, but also reduces the computational complexity after training, which lays a good foundation for the subsequent model iteration and application.

V. Discussion

In the above experimental results, the improved DCGAN model has a good performance and has obvious advantages in the field of image restoration. Therefore, this method also has certain application potential in other fields. In medical imaging, medical imaging technology is highly dependent on image quality. Images are often distorted by noise, motion artifacts, or equipment limitations. By applying the improved DCGAN model, damaged medical images can be effectively restored, enhancing the contrast and detail of the images, thereby helping doctors obtain more accurate diagnoses. DS-DCGAN can be used to process noise reduction and enhance image quality, improving the recognition and classification accuracy of pathology images, which is essential for early diagnosis. In medical image analysis, DS-DCGAN can be used to generate diverse training samples, help train other deep learning models, and promote the accuracy of cancer lesion detection or tissue classification. By generating high-quality composite images, the sample pool can be increased, helping to reduce overfitting and training time for the model. Medical imaging systems usually produce a large number of scanned images. As time goes on, storing and managing these images becomes increasingly important. DS-DCGAN can help digitally preserve expired and damaged medical images, making important historical medical records and records continuously accessible and usable.

In terms of digital heritage protection, many important historical documents, artworks and images of cultural assets face wear and degradation. DS-DCGAN can be used to effectively repair these damaged images, improve their visual effect, and help retain historical information and cultural memory. The improved DCGAN model can be applied in 3D reconstruction to generate 3D assets with a high degree of detail by restoring flat images. In addition, this restoration method can be combined with augmented reality technology to provide visitors with a more vivid experience of cultural heritage. In a virtual museum or exhibition, DS-DCGAN is capable of recreating historical scenes to provide a more immersive and informative presentation.

In other potential areas, such as in film and television post-production, it is often necessary to recover damaged footage or enhance the details of a scene. DS-DCGAN helps production teams quickly fix scenes and generate additional effects, saving processing time and money. In security monitoring, the images captured by cameras are often difficult to provide effective information because of insufficient illumination and blurred motion. DS-DCGAN applications improve the clarity of surveillance images and help analyze and identify potential security threats. In the intelligent traffic management system, DS-DCGAN can optimize traffic monitoring images and recover important road condition information. This can enhance the real-time processing of images and optimize the management and control of traffic flow.

VI. Conclusion

In order to effectively restore landscape design images, a landscape design image restoration model was constructed by combining DenseNet, SENet, and DCGAN. Compared with DCGAN, GAN-variant, and CGAN, the results showed that DS-DCGAN maintained stability after 216 iterations in the training set and 172 iterations in the testing set, with faster iteration speed. In addition, the MSE and MAE of DS-DCGAN were the smallest in stable state, which were 0.08 and 0.07, respectively, indicating that the algorithm had low error. The repair accuracy and recall rate of four algorithms were tested. It was found that the repair precision and recall rate of DS-DCGAN were both as high as 0.97, indicating that this method could better preserve the detailed information during the repair process. In practical applications, the average repair accuracy of this model was as high as 99.03%, and the average repair time was as low as 0.06s. From this, the proposed DS-DCGAN model has good repair performance and application effectiveness. By introducing an improved DCGAN model and combining DenseNet and SENet, a new approach is provided to process and restore landscape design images. This method not only improves the ability of feature extraction, but also significantly improves the accuracy and efficiency of image recovery. The implementation and results of the research will have a profound impact on related fields. Landscape design image restoration can provide more accurate data support for urban planning and management, and help decision makers to better carry out land planning, environmental management and public facilities layout. It provides a new methodology and direction for the field of image restoration, promotes academic accumulation in the field, and promotes the expansion of subsequent research into more complex and diverse image processing tasks. At the same time, due to the complexity of landscape design images and the diversity of their damage types, subsequent research can analyze more types of damaged image restoration. As a result, follow-up studies can add repair analysis for more types of damaged images. At the same time, multiple approaches can be explored to further generalize and adapt the DS-DCGAN model to different types of image restoration tasks. For example, exploring the application of DS-DCGAN to multimodal image restoration, such as combining different types of medical imaging to achieve more comprehensive image restoration; DS-DCGAN is extended to video processing and dynamic scene recovery to improve the image quality under the condition of motion blur and motion

artifact. DS-DCGAN is applied to super-resolution reconstruction tasks, especially scenarios where high-resolution images are recovered from low-resolution images. By exploring these directions in depth, the DS-DCGAN model can not only meet the needs of challenging image restoration, but also show greater value in diverse fields.

REFERENCES

[1] Yang G, Wei W, Pan Z. A Variational neural network for image restoration based on coupled regularizers. Multimedia Tools and Applications, 2024, 83(4): 12379-12401.

[2] Luo Q, Liao Y, Jing B, Gao X, Chen W, Tan K. Hir-net: a simple and effective heterogeneous image restoration network. Signal, Image and Video Processing, 2024, 18(1): 773-784.

[3] Saminu S, Xu G, Zhang S, Kader IAE, Aliyu HA, Jabire AH, Ahmed YK, Adamu MJ. Applications of Artificial Intelligence in Automatic Detection of Epileptic Seizures Using EEG Signals: A Review. Artificial Intelligence and Applications, 2023, 1(1): 11-25.

[4] Mao L, Wang M, Yang D, Zhang R. Mutual learning generative adversarial network. Multimedia Tools and Applications, 2024, 83(3): 7479-7503.

[5] Skandarani Y, Lalande A, Afilalo J, Jodoin P M. Generative adversarial networks in cardiology. Canadian Journal of Cardiology, 2022, 38(2): 196-203.

[6] Pan J, Dong J, Liu Y, Zhang J, Ren J, Tang J, Yang M H. Physics-based generative adversarial models for image restoration and beyond. IEEE transactions on pattern analysis and machine intelligence, 2020, 43(7): 2449-2462.

[7] Liu G, Li X, Wei J. Large-area damage image restoration algorithm based on generative adversarial network. Neural Computing and Applications, 2021, 33(10): 4651-4661.

[8] Deng Z, Cai Y, Chen L, Gong Z, Bao Q, Yao X, Ma L. Rformer: Transformer-based generative adversarial network for real fundus image restoration on a new clinical benchmark. IEEE Journal of Biomedical and Health Informatics, 2022, 26(9): 4645-4655.

[9] Yang J, Liu J, Han R, Wu J. Generating and restoring private face images for internet of vehicles based on semantic features and adversarial examples. IEEE Transactions on Intelligent Transportation Systems, 2021, 23(9): 16799-16809.

[10] Ma H, Liu D, Wu F. Rectified wasserstein generative adversarial networks for perceptual image restoration. IEEE Transactions on Pattern Analysis and Machine Intelligence, 2022, 45(3): 3648-3663.

[11] Kumar P, Gupta V. Restoration of damaged artworks based on a generative adversarial network. Multimedia Tools and Applications, 2023, 82(26): 40967-40985.

[12] Liang M, Zhang Q, Wang G, Xu N, Wang L, Liu H, Zhang C. Multi-scale self-attention generative adversarial network for pathology image restoration. The Visual Computer, 2023, 39(9): 4305-4321.

[13] Pan X, Zhan X, Dai B, Lin D, Loy C C, Luo P. Exploiting deep generative prior for versatile image restoration and manipulation. IEEE Transactions on Pattern Analysis and Machine Intelligence, 2021, 44(11): 7474-7489.

[14] Mitrofanov E, Grishkin V. Generative Adversarial Networks Quantization. Physics of Particles and Nuclei, 2024, 55(3): 563-565.

[15] Chen Y, Gao Q, Wang X. Inferential Wasserstein generative adversarial networks. Journal of the Royal Statistical Society Series B: Statistical Methodology, 2022, 84(1): 83-113.

[16] Alghazzawi D M, Hasan S H, Bhatia S. Optimized Generative Adversarial Networks for Adversarial Sample Generation. Computers, Materials & Continua, 2022, 72(2): 3877-3897.

[17] Zhang J, Dong Q, Song W. GGADN: Guided generative adversarial dehazing network. Soft Computing, 2023, 27(3): 1731-1741.

[18] Jafari A, Al-Mousa A, Jafar I. Speaker anonymization using generative adversarial networks. Journal of Intelligent & Fuzzy Systems, 2023, 45(2): 3345-3359.

[19] Kumar P, Gupta V. Restoration of damaged artworks based on a generative adversarial network. Multimedia Tools and Applications, 2023, 82(26): 40967-40985.